High Power Laser Science and Engineering, (2022), Vol. 10, e35, 7 pages.
doi:10.1017/hpl.2022.21

HIGH POWER LASER SCIENCE AND ENGINEERING

RESEARCH ARTICLE

High laser damage threshold reflective optically addressed liquid crystal light valve based on gallium nitride conductive electrodes

Zhibo Xing[1,2], Wei Fan[1,2], Dajie Huang[1], He Cheng[1], and Tongyao Du[1]

[1] *National Laboratory on High Power Laser and Physics, Shanghai Institute of Optics and Fine Mechanics, Chinese Academy of Sciences, Shanghai, China*

[2] *Center of Materials Science and Optoelectronics Engineering, University of Chinese Academy of Sciences, Beijing, China*

(Received 7 March 2022; revised 2 July 2022; accepted 18 August 2022)

Abstract

In this paper, the feasibility of a high laser damage threshold liquid crystal spatial light modulator based on gallium nitride (GaN) transparent conductive electrodes is proved. The laser-induced damage threshold (LIDT) is measured, and a high LIDT reflective optically addressed liquid crystal light valve (OALCLV) based on GaN is designed and fabricated. The proper work mode of the OALCLV is determined; the OALCLV obtained a maximum reflectivity of about 55% and an on–off ratio of 55:1, and an image response is demonstrated.

Keywords: gallium nitride; laser-induced damage threshold; liquid crystal; optically addressed liquid crystal light valve

1. Introduction

The liquid crystal spatial light modulator (LC-SLM), as an optical device that can control the amplitude, phase and polarization of the light field in real time, has important applications in military, medical, industrial and other fields[1–4].

The LC-SLM plays an important role in beam quality control of large-scale laser devices, and is used for beam intensity pre-compensation, pre-shielding of damage points and improving beam intensity uniformity[5–8]. Among LC-SLMs, the optically addressed liquid crystal light valve (OALCLV) is a kind of spatial light modulator without a pixel electrode, compared with the transmittance spatial light modulator based on thin film transistors (TFTs) and the reflective spatial light modulator based on liquid crystal on silicon (LCoS). It not only avoids the low opening rate of the TFT spatial light modulator caused by non-transparent electrodes and other components[9], but also avoids the optical path distortion caused by the black-matrix effect of the LCoS spatial light modulator[5], which has a relatively large advantage in the application of the LC-SLM in large-scale laser devices. Until now, the OALCLV has been used for beam shaping in the National Ignition Facility (NIF) in the USA[10], the Laser Megajoule (LMJ) in France[11] and the 'Shenguang' serials in China[6,7].

With the development and increasing application requirements of high-power lasers, their application scenarios have higher requirements on the laser-induced damage threshold (LIDT) of the OALCLV, which poses a challenge to the improvement of laser damage resistance of existing OALCLVs. In the existing OALCLV, its LIDT is mainly restricted by the laser damage resistance of the material of its transparent conductive film, while the existing indium tin oxide (ITO) is unable to meet the requirements of the high LIDT in high-power laser systems.

It is reported[12] that the LIDT of transparent conductive films can be improved by using gallium nitride (GaN) instead of ITO as the transparent conductive material. At present, we have verified the feasibility of GaN as a transparent conductive material of LC-SLMs, and have made liquid crystal switches based on GaN transparent conductive films[13].

This paper will focus on the application of GaN in OALCLVs. By using GaN as the transparent conductive material of reflective OALCLVs, the hybrid field effect (HFE) reflective amplitude-only high LIDT OALCLV based on GaN is designed and fabricated, and its working mode is deter-

Correspondence to: W. Fan, National Laboratory on High Power Laser and Physics, Shanghai Institute of Optics and Fine Mechanics, Chinese Academy of Sciences, 390 Qinghe Road, Jiading District, Shanghai 201800, China. Email: fanweil@siom.ac.cn

mined. The obtained reflective OALCLV achieves a good extinction ratio and graphic response performance.

2. Theory and experiment setup

The basic structure of the reflective OALCLV is shown in Figure 1, in which the voltage is loaded to the series-wound liquid crystal layer and bismuth silicon oxide (BSO) photoconductive layer through the GaN transparent conductive layer and ITO conductive layer, and the address light irradiates to the BSO photoconductive layer from the LCoS input and is reflected by the reflective layer. The resistance distribution of the BSO layer is adjusted through the photoconductive effect of the BSO layer, and the voltage distribution of the liquid crystal layer is adjusted. The readout light irradiates to the liquid crystal cell after polarizing, and is reflected by the reflective layer after the modulation by the liquid crystal cell. In the liquid crystal cell, the GaN layer is coated with an anti-reflection layer to improve its transmittance from 70%–80%[13] to over 90%, and the liquid crystal layer is aligned by polyimide layers on the two substrates. After the modulation by the liquid crystal cell, the polarization of the readout light is rotated by 90°, and the readout light is reflected to a vertical direction through the polarization beam splitter (PBS). Through a second polarizer, as an analyzer that is vertical to the first polarizer, the intensity of the readout light is modulated and output to the image sensor.

For reflective LC-SLMs represented by the LCoS, its working modes include the electronically controlled birefringence (ECB) mode, twisted-nematic electronically controlled birefringence (TN-ECB) mode, mixed twisted-nematic (MTN) mode, self-compensating twisted-nematic (SCTN) mode, HFE mode[14–16], etc. Considering the amplitude modulation requirement of beam shaping in large-scale laser devices, the HFE mode was selected. In this mode, the twist angle between the upper and lower substrates of the liquid crystal is 45° or 52°–54°. Considering the process conditions, the twist angle is selected as 45°. In this case, the thickness of the cell should meet $d\Delta n = \frac{\sqrt{15}}{4}\lambda$[14], where d is the thickness of the cell, Δn is the birefringence of the liquid crystal and λ is the wavelength of the readout light.

For the HFE mode, some research achievements have been made on its off-state static voltage relationship, but there is a lack of research on its dynamic voltage response after the voltage is loaded. In order to determine the driving conditions of the reflective OALCLV, the voltage response of the HFE liquid crystal cell is simulated. The off-state reflectivity used in the simulation is the actual experimental data of the OALCLV fabricated based on the structure in Figure 1. The data is measured by a CinCam CMOS-1202 beam profiler and determined from the ratio of the integral intensity between the off-state output after modulation of the OALCLV and the input light. The on-state reflectivity and the average on–off state ratio are also measured by a similar method. The simulation conditions and results are shown in Table 1 and Figure 2, respectively.

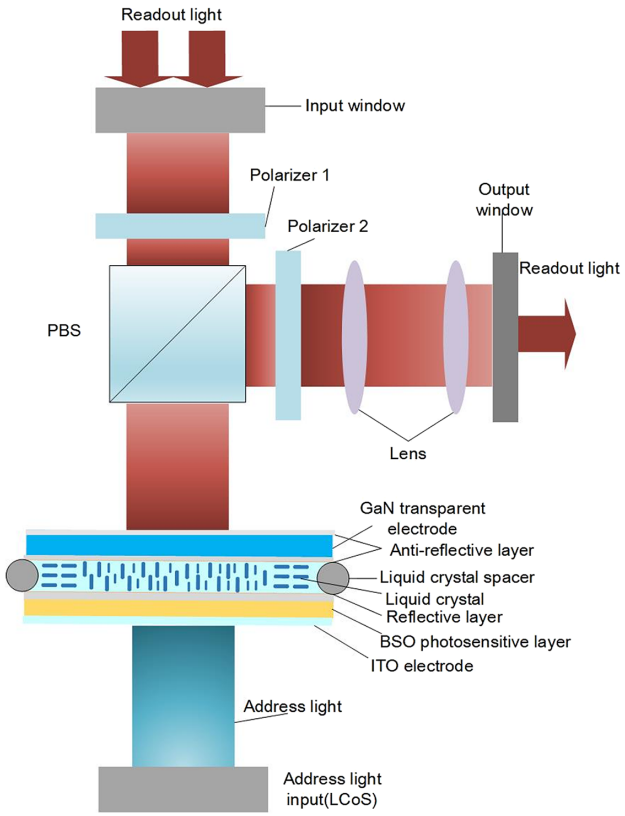

Figure 1. The basic structure of the reflective OALCLV.

It is shown that for HFE cells, different from the twisted-nematic (TN) mode of the transmission liquid crystal cells[13], there is an optimal driving voltage of the liquid crystal layer, beyond which the switching ratio will gradually decrease. According to Figure 2, the optimal driving voltage of the liquid crystal layer is about 1.009 V.

For liquid crystal cells based on a BSO photoconductive layer, the relationship between the liquid crystal layer voltage and the driving voltage of the full liquid crystal cell is as follows:

$$V_{\mathrm{LC}} = V_{\mathrm{AC}} \cdot \frac{\frac{1}{R_0} + \frac{1}{R_\Phi} + j\omega C_{\mathrm{BSO}} + \frac{j\omega C_1}{1+j\omega R_1 C_1}}{\frac{1}{R_0} + \frac{1}{R_\Phi} + j\omega C_{\mathrm{BSO}} + \frac{j\omega C_1}{1+j\omega R_1 C_1} + \frac{1}{R_{\mathrm{LC}}} + j\omega C_{\mathrm{LC}}}, \tag{1}$$

Table 1. The parameters in the simulation of the HFE mode reflective liquid crystal cell.

Conditions	Value
Wavelength (λ)	1053 nm
Ordinary refractive index (n_o)	1.517
Extraordinary refractive index (n_e)	1.741
Thickness of the cell	4.6 μm
Off-state reflectivity	1%

https://doi.org/10.1017/hpl.2022.21 Published online by Cambridge University Press

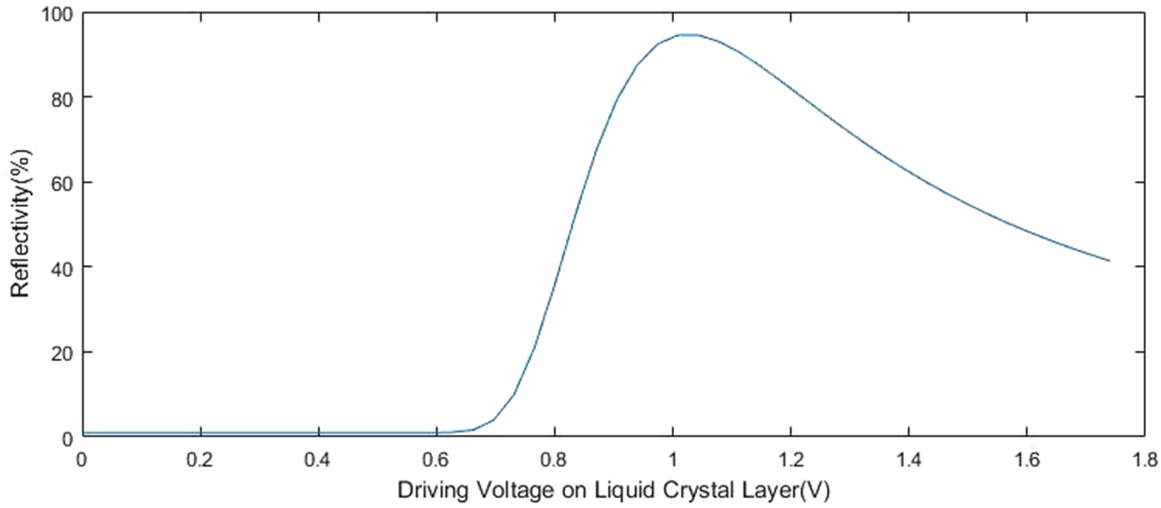

Figure 2. The relationship between the driving voltage on the liquid crystal cell and the reflectivity of the OALCLV. Only the loss of the liquid crystal layer is considered; the other layers are considered as ideal materials.

where V_{AC} represents the amplitude of the driving voltage on the liquid crystal cell, V_{LC} represents the partial voltage on the liquid crystal layer, R_{LC}, C_{LC} are the resistance and capacitance of the liquid crystal layer, respectively, R_0 is the dark resistance of BSO and R_Φ is the resistance of the BSO photosensitive layers being illuminated, which is determined by Equation (2)[17]:

$$R_\Phi = \frac{1}{U(\alpha)I}. \tag{2}$$

in which $U(\alpha)$ is the photoconductivity constant of BSO and I is the illumination intensity on the BSO layer. C_{BSO} is the capacitance of the BSO layer itself, R_1, C_1 are the resistance and capacitance caused by the bound charge of the BSO layer, respectively, and ω represents the circular frequency of the driving voltage, which meets the relationship with the driving frequency $\omega = 2\pi f$. The relevant parameters are shown in Table 2.

By substituting other parameters, the above equation can be regarded as a relationship between the voltage ratio of the liquid crystal layer and the liquid crystal cell and the driving frequency of the liquid crystal cell. For the above equation, the specific frequency and the light intensity parameters in the actual experiment are plugged in, and the results are shown in Figure 3.

It is shown in Figure 3 that the voltage ratio of the liquid crystal layer in the off-state is less affected by the driving frequency than that in the on-state. Therefore, the actual total driving voltage and driving frequency of the liquid crystal cell are mainly determined by the condition of the voltage ratio in the off-state. According to Figure 2, the maximum voltage to keep the off-state of the liquid crystal cell is 0.627 V, considering that a low driving frequency will cause the instability of the image output of the liquid crystal cell,

Table 2. The parameters of the liquid crystal cell in Equation (1).

Parameter	Value
R_{LC}	1.15×10^{6} Ω[18]
C_{LC}	1.286×10^{-8} F
R_0	1.25×10^{12} Ω[18]
C_{BSO}	1.98×10^{-10} F[18]
R_1	6×10^{6} Ω[18]
C_1	1.2×10^{-10} F[18]
R_Φ (light mode)	2.14×10^{6} Ω
R_Φ (dark mode)	1.07×10^{8} Ω

while in the Figure 3(b) the voltage of the liquid crystal layer and the driving frequency are positively associated; hence, in order to guarantee the imaging performance of the liquid crystal cell, the ideal off-state voltage of the liquid crystal layer should be close to but not larger than the value of 0.627 V. Therefore, according to Figure 3(a), in the range of 100–1000 Hz (a driving frequency beyond this range will influence the normal working of the liquid crystal cell), V_{AC}/V_{LC} is about 42–59, which means that the maximum driving voltage should be between 26 and 37 V. In experimental measurements, the driving voltage of the actual liquid crystal cell to achieve the lowest off-state reflectance is 27 V, and the best driving frequency of the liquid crystal cell is 208 Hz.

3. Experimental results

In order to verify the performance of the reflective OALCLV based on the GaN transparent conductive layer, a reflective OALCLV based on GaN is fabricated, and its structure is shown in Figure 1. Considering the problem of uneven thickness of the GaN liquid crystal cell[13] previously made due to the thin substrate thickness of the GaN layer, a

https://doi.org/10.1017/hpl.2022.21 Published online by Cambridge University Press

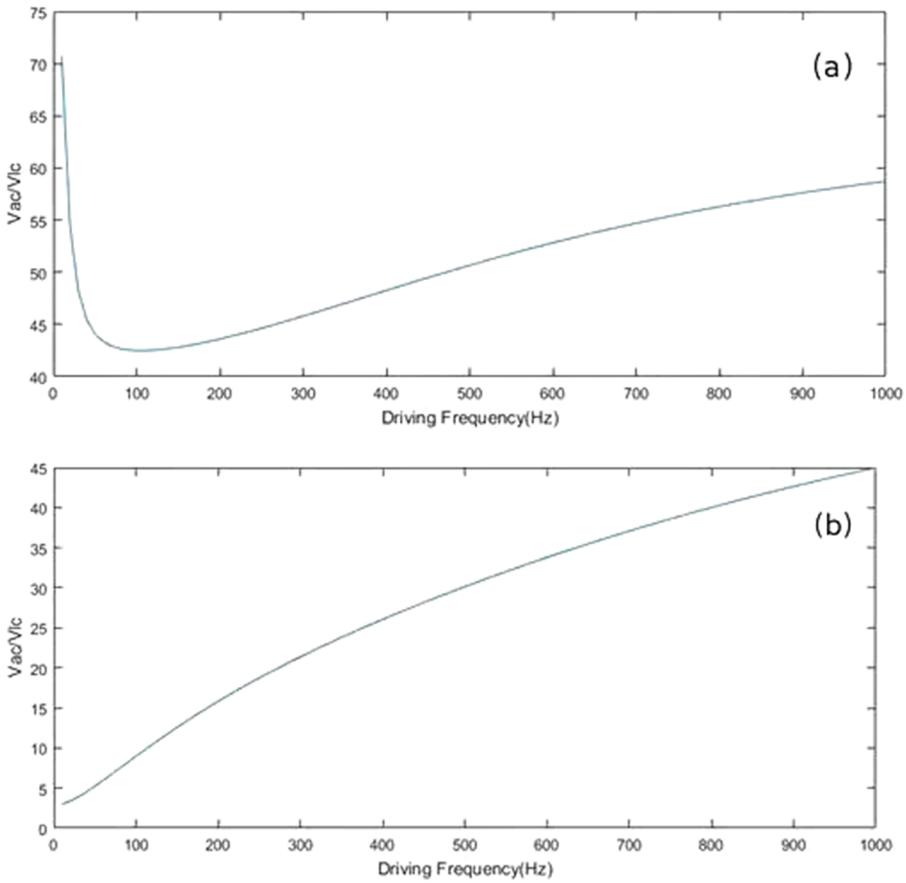

Figure 3. The relationship between the ratio of the voltage of the liquid crystal layer and the total voltage and the driving frequency in the (a) off-state and (b) the on-state.

14 mm × 15 mm × 1 mm silicon-doped GaN single crystal is used in the new liquid crystal cell. The thickness of the liquid crystal cell is 4.6 μm, and the overall size of the reflective OALCLV based on GaN is about 14 mm × 15 mm × 2 mm.

Although the nanosecond damage threshold of GaN based on the sapphire substrate has been measured as about 1.67 J/cm^2 [13], which indicates the high LIDT potential of GaN material, the laser damage ability of the GaN single crystal has not been verified. In order to verify the feasibility of the GaN single crystal as a transparent conductive material with high LIDT, an LIDT test was conducted on the GaN single crystal. The test facility is shown in Figure 4. As shown in Figure 4, the pulse Gaussian laser with a circular spot is adjusted by an energy attenuator consisting of a half waveplate and a polarizer. Through the focusing lens, the energy and the effective area of the beam spot are respectively measured by an energy meter and a beam analyzer. The damage sites are illuminated by a He-Ne laser, which is collinear with the pulse beam, and then detected by an online charge-coupled device (CCD) camera after the focus lens. The parameters in the experimental setup are shown in Table 3. There are in total 70 effective damage sites available on the GaN sample, and seven pulse energies are selected. For each selected pulse energy, 10 damage sites are exposed. The result of the test is shown in Figure 5. At 3.06 J/cm^2, the damage probability is shown as 0%, indicating an LIDT over 3.06 J/cm^2 for the GaN single crystal. On the other hand, the fitting data show a damage probability of 0% at about 1.23 J/cm^2, which is also larger than the LIDT of the conventional ITO layer[13]. The damage spot micrograph of the GaN specimen is detected by a digital microscope, VHX-6000, and the result is shown in Figure 6.

The performance of the newly fabricated reflective liquid crystal cell was measured. The readout laser is 1053 nm. The main light path diagram is shown in Figure 1. A computer was connected with the LCoS, and the readout signal light was adjusted by the method of changing the computer input image. The off and on states of the liquid crystal cell were determined by loading total black and total white images on the LCoS, respectively, so as to obtain the maximum reflectivity, on–off ratio and response speed of the liquid crystal cell. The output image is detected by a CinCam CMOS-1202 beam profiler. The on-state reflectivity is determined from the ratio of the integral intensity

https://doi.org/10.1017/hpl.2022.21 Published online by Cambridge University Press

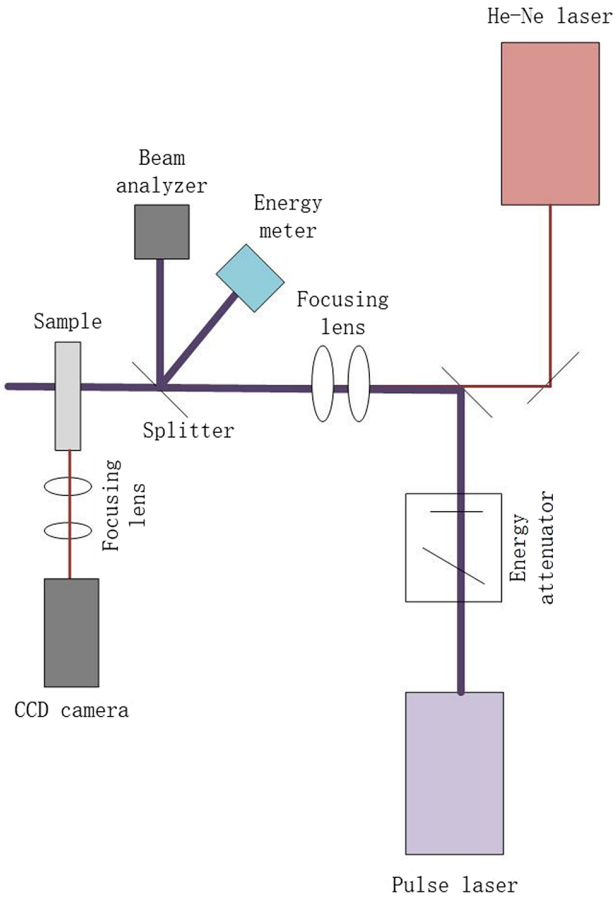

Figure 4. Schematic of the experimental facility used for the GaN damage resistance test.

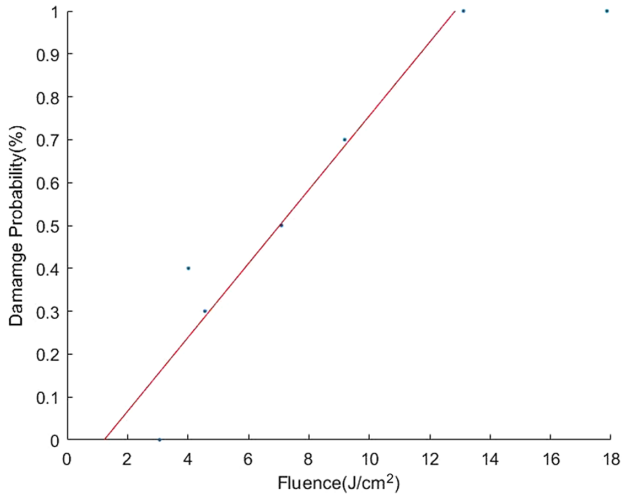

Figure 5. The laser damage data of the GaN single crystal. The experimental data of the damage probability are represented by discrete points, while the fitting data are represented by the linear fitting line.

Figure 6. The damage spot micrograph of the GaN single crystal specimen (the measuring scale is shown in the figure).

detected on the beam profiler between the on-state output and the input light, and the on–off ratio is determined by the ratio of the on-state reflectivity and the off-state reflectivity, which is shown in Table 1. The test conditions and results are shown in Table 4 and Figure 7. As shown in the table, the performance of the liquid crystal cell, especially the on–off ratio, determined by the ratio of the whole integral intensity between the on-state output and off-state output detected by the beam profiler, achieves a maximum value of about 55:1. The response speed of the OALCLV is tested using a Tektronix TDS360 oscilloscope, in which the rising edge and declining edge are both about 100 ms, which is shown in Figure 8.

Table 3. The parameters in the damage resistance test of the GaN single crystal.

Parameter	Value
Wavelength	1053 nm
Pulse width	12 ns
Test type	1-on-1
Effective area of the spot	0.1 mm^2
Total damage sites	70

In order to verify the performance of the reflective liquid crystal cell as an OALCLV, the image response of the reflected liquid crystal cell was tested by loading the image on the OALCLV. The test results are shown in Figure 9. As shown in the figure, the image can be well transmitted to the readout light by the OALCLV.

Table 4. The experimental setup and result of the reflective OALCLV.

Conditions/results	Value
Readout wavelength	1053 nm
Input pulse width	12 ns
Wavelength of the address light	470 nm
Driving voltage	27 V
Driving frequency	208 Hz
Maximum reflectivity	55%
Average maximum on–off ratio	~55
Response speed	~100 ms (up/down)

https://doi.org/10.1017/hpl.2022.21 Published online by Cambridge University Press

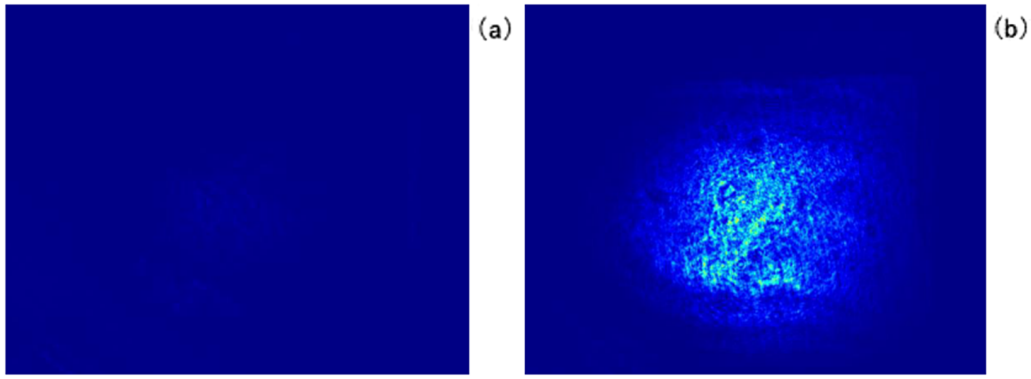

Figure 7. The image response of full black input (a) and full white input (b) of the OALCLV.

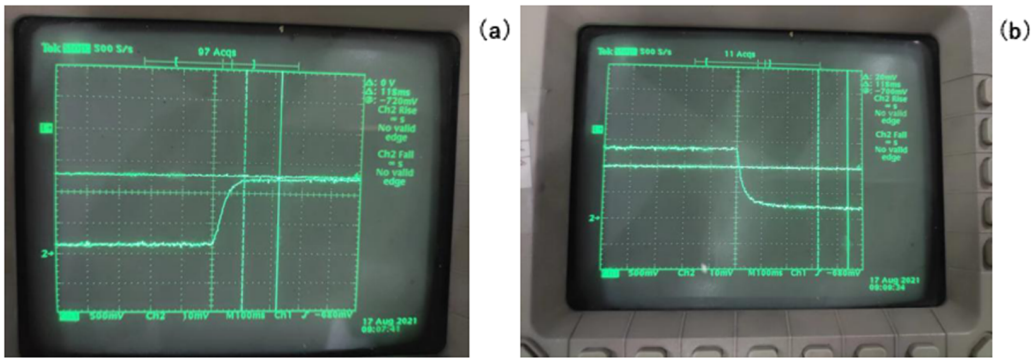

Figure 8. The test result (rising curve (a) and declining curve (b)) of the response speed of the OALCLV.

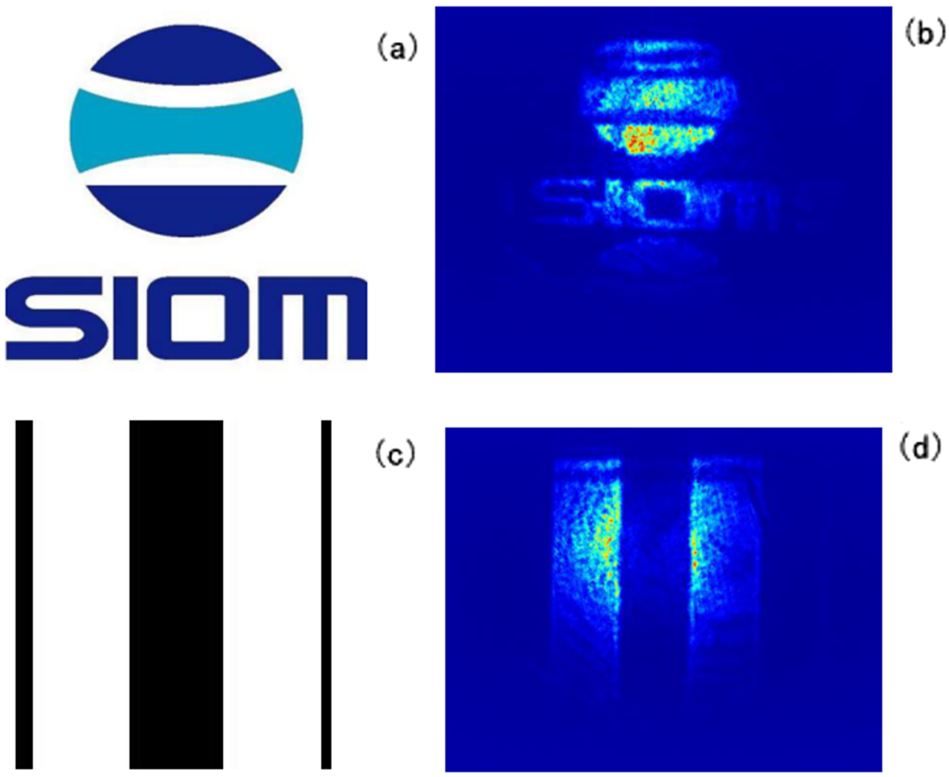

Figure 9. The image response test result of the reflective OALCLV: input ((a), (c)) and output ((b), (d)).

https://doi.org/10.1017/hpl.2022.21 Published online by Cambridge University Press

4. Conclusion

In this paper, the feasibility of a high laser damage resistance reflective OALCLV based on transparent conductive material, GaN, is verified. In order to determine the driving conditions of the reflective OALCLV, the voltage response of the used HFE mode is simulated. Under the required driving conditions, the GaN-based reflective OALCLV obtained a maximum reflectivity of about 55% and average on–off ratio of 55:1, and an image response is demonstrated. The results confirm that the GaN-based reflective OALCLV has a good performance as a light-addressing LC-SLM, and it is expected that LC-SLMs with high laser damage resistance can be obtained by GaN transparent conductive layers.

For the high damage threshold LC-SLM based on the GaN transparent electrode, a great development prospect can be foreseen. Considering that reflective LC-SLMs still introduce reflective devices into the original light path, which may have an influence on the laser system, the development of the transmitted LC-SLM based on GaN may be the next focus of high laser damage resistance LC-SLMs based on GaN.

Acknowledgments

The authors gratefully acknowledge the laser damage measurement of the Thin Film Optics Laboratory at the Shanghai Institute of Optics and Fine Mechanics, Chinese Academy of Sciences and the support of the Research Center for Laser Intelligent Manufacturing at the Shanghai Institute of Optics and Fine Mechanics, Chinese Academy of Sciences.

Funding

This work was supported by the Strategic Priority Research Program of the Chinese Academy of Sciences (No. XDA25020303).

References

1. S. Tonda-Goldstein, D. Dolfi, A. Monsterleet, S. Formont, J. Chazelas, and J. P. Huignard, IEEE Trans. Microwave Theory Tech. **54**, 847 (2006).
2. S. A. Vasquez-Lopez, R. Turcotte, V. Koren, M. Plöschner, Z. Padamsey, M. J. Booth, T. Čižmár, and N. J. Emptage, Light Sci. Appl. **7**, 1 (2018).
3. M. J. Matthews, G. Guss, D. R. Drachenberg, J. A. Demuth, J. E. Heebner, E. B. Duoss, J. D. Kuntz, and C. M. Spadaccini, Opt. Express **25**, 11788 (2017).
4. Y. Cai, D. Huang, H. Cheng, G. Xia, and W. Fan, Appl. Sci. **11**, 3647 (2021).
5. D. Huang, W. Fan, H. Cheng, G. Xia, L. Pei, X. Li, and Z. Lin, High Power Laser Sci. Eng. **6**, e20 (2018).
6. D. Huang, W. Fan, X. Li, and Z. Lin, Chin. Opt. Lett. **11**, 072301 (2013).
7. D. Huang, W. Fan, X. Li, and Z. Lin, Chin. Opt. Lett. **10**, S21406 (2012).
8. D. Huang, W. Fan, X. Li, and Z. Lin, Proc. SPIE **8556**, 855615 (2012).
9. M. Katayama, Thin Solid Films **341**, 140 (1999).
10. J. Heebner, M. Borden, P. Miller, S. Hunter, K. Christensen, M. Scanlan, C. Haynam, P. Wegner, M. Hermann, G. Brunton, E. Tse, A. Awwal, N. Wong, L. Seppala, M. Franks, E. Marley, K. Williams, T. Budge, M. Henesian, C. Stolz, T. Suratwala, M. Monticelli, D. Walmer, S. Dixit, C. Widmayer, J. Wolfe, J. Bude, K. McCarty, and J. M. DiNicola, Proc. SPIE **7916**, 79160H (2011).
11. J. Luce, Proc. SPIE **8130**, 813002 (2011).
12. S. Elhadj, "Next-generation films for high-performance optoelectronics applications," LDRD Annual Report (2017).
13. Z. Xing, W. Fan, D. Huang, H. Cheng, and G. Xia, Opt. Lett. **45**, 3537 (2020).
14. S. Reichelt, Appl. Opt. **52**, 2610 (2013).
15. T. Sonehara, Jpn. J. Appl. Phys. **29**, L1231 (1990).
16. M. Lu, J. Soc. Inform. Display **10**, 37 (2002).
17. T. Wang and S. Xu, Chin. J. Lasers **11**, 483 (1984).
18. P. Aubourg, J. P. Huignard, M. Hareng, and R. A. Mullen, Appl. Opt. **21**, 3706 (1982).

https://doi.org/10.1017/hpl.2022.21 Published online by Cambridge University Press